SUPPLEMENTARY INFORMATION

Supplementary Information for "Fundamental and higher eigenmodes of qPlus sensors with a long probe for vertical-lateral bimodal atomic force microscopy"

Yuya Yamada,[a] Takashi Ichii,[a*] Toru Utsunomiya,[a] Kuniko Kimura,[b] Kei Kobayashi,[b] Hirofumi Yamada[b] and Hiroyuki Sugimura[a]

The supplementary information contents:

S1. Details of theoretical analysis of the eigenmodes

S2. FEM results

S3. Sensor characterization

S4. Bimodal AFM results

[a] *Department of Materials Science and Engineering, Kyoto University, Yoshida Honmachi, Sakyo, Kyoto 606-8501, Japan.*

[b] *Department of Electronic Science and Engineering, Kyoto University, Katsura, Nishikyo, Kyoto 615-8510, Japan.*

S1 Details of theoretical analysis of the eigenmodes

The total kinetic energy T and potential energy U of a qPlus sensor are given by Eq. 1 shown in the text. Using Eq. 1 along with Hamilton's principle, we obtain the equations of motion for free undamped oscillations,

$$E_q I_q \frac{\partial^4 w}{\partial x_1^4}(x_1,t) + \rho_q A_q \ddot{w}(x_1,t) = 0, \tag{S1a}$$

$$E_w I_w \frac{\partial^4 u}{\partial x_2^4}(x_2,t) + \rho_w A_w \left(\ddot{u}(x_2,t) + \left(x_2 + \frac{h}{2}\right) \frac{\partial \ddot{w}}{\partial x_1}(L,t) \right) = 0, \tag{S1b}$$

and the boundary conditions for the QTF prong,

$$w(0,t) = 0, \tag{S2a}$$

$$\frac{\partial w}{\partial x_1}(0,t) = 0, \tag{S2b}$$

$$E_q I_q \frac{\partial^3 w}{\partial x_1^3}(L,t) - M_{probe} \left(\ddot{w}(L,t) + \frac{d}{2} \frac{\partial \ddot{w}}{\partial x_1}(L,t) \right) = 0, \tag{S2c}$$

$$\begin{aligned} -E_q I_q \frac{\partial^2 w}{\partial x_1^2}(L,t) - \frac{d}{2} M_{probe} \left(\ddot{w}(L,t) + \frac{d}{2} \frac{\partial \ddot{w}}{\partial x_1}(L,t) \right) - I_a \frac{\partial \ddot{w}}{\partial x_1}(L,t) \\ -I_c \left(\frac{\partial \ddot{w}}{\partial x_1}(L,t) + \frac{\partial \ddot{u}}{\partial x_2}(l_b,t) \right) + \int_0^{l_b} -\rho_w A_w \left(x_2 + \frac{h}{2} \right) \left(\ddot{u}(x_2,t) + \left(x_2 + \frac{h}{2} \right) \frac{\partial \ddot{w}}{\partial x_1}(L,t) \right) dx_2 \\ - \left(l_b + \frac{h}{2} + \frac{1}{4} l_c \right) M_c \left(\ddot{u}(l_b,t) + \frac{1}{4} l_c \frac{\partial \ddot{u}}{\partial x_2}(l_b,t) + \left(l_b + \frac{h}{2} + \frac{1}{4} l_c \right) \frac{\partial \ddot{w}}{\partial x_1}(L,t) \right) = 0, \end{aligned} \tag{S2d}$$

and the boundary conditions for the tungsten needle,

$$u(0,t) = 0, \tag{S3a}$$

$$\frac{\partial u}{\partial x_2}(0,t) = 0, \tag{S3b}$$

$$E_w I_w \frac{\partial^3 u}{\partial x_2^3}(l_b,t) - M_c \left(\ddot{u}(l_b,t) + \frac{1}{4} l_c \frac{\partial \ddot{u}}{\partial x_2}(l_b,t) + \left(l_b + \frac{h}{2} + \frac{1}{4} l_c \right) \frac{\partial \ddot{w}}{\partial x_1}(L,t) \right) = 0, \tag{S3c}$$

$$
\begin{aligned}
&-E_w I_w \frac{\partial^2 u}{\partial x_2^2}(l_b,t) - I_c\left(\frac{\partial \ddot{w}}{\partial x_1}(L,t) + \frac{\partial \ddot{u}}{\partial x_2}(l_b,t)\right) \\
&-\frac{1}{4}M_c\left(\ddot{u}(l_b,t) + \frac{1}{4}l_c\frac{\partial \ddot{u}}{\partial x_2}(l_b,t) + \left(l_b + \frac{h}{2} + \frac{1}{4}l_c\right)\frac{\partial \ddot{w}}{\partial x_1}(L,t)\right) = 0,
\end{aligned}
\tag{S3d}
$$

As the global displacement of the tungsten needle, $v(x_2,t) = u(x_2,t) + \left(x_2 + \frac{h}{2}\right)\frac{\partial w}{\partial x_1}(L,t)$, is induced under an assumption that the bending displacements of the beams and the gradient at the end of the QTF prong are small ($w(x_1,t), u(x_2,t) \ll h$ and $\frac{\partial w}{\partial x_1}(L,t) \ll 1$), the equations of motion and boundary conditions change into the form of Eqs. 2-4 shown in the text. Using the method of separation of variables, the solutions of the displacements of the QTF prong and tungsten needle are assumed as $w(x_1,t) = \exp(i\omega t)\Phi(x_1)$ and $v(x_2,t) = \exp(i\omega t)\Psi(x_2)$, where $\exp(i\omega t)$ is the temporal component of the solution with an angular frequency ω, and $\Phi(x_1)$ and $\Psi(x_2)$ are the spatial components of the solution. By substituting the solutions of the displacements into Eq. S1 and eliminating the temporal component, the equations of the spatial components are given below:

$$
\frac{\partial^4 \Phi}{\partial x_1^4}(x_1) = \frac{\omega^2 \rho_q A_q}{E_q I_q}\Phi(x_1), \tag{S4a}
$$

$$
\frac{\partial^4 \Psi}{\partial x_2^4}(x_2) = \frac{\omega^2 \rho_w A_w}{E_w I_w}\Psi(x_2). \tag{S4b}
$$

Then, the general solutions of $\Phi(x_1)$ and $\Psi(x_2)$ are given by,

$$
\begin{aligned}
&\Phi(x_1) = C_1\sin(\alpha x_1) + C_2\cos(\alpha x_1) + C_3\sinh(\alpha x_1) + C_4\cosh(\alpha x_1), \\
&\alpha = \sqrt[4]{\frac{\omega^2 \rho_q A_q}{E_q I_q}},
\end{aligned}
\tag{S5a}
$$

$$
\begin{aligned}
&\Psi(x_2) = D_1\sin(\beta x_2) + D_2\cos(\beta x_2) + D_3\sinh(\beta x_2) + D_4\cosh(\beta x_2), \\
&\beta = \sqrt[4]{\frac{\omega^2 \rho_w A_w}{E_w I_w}}.
\end{aligned}
\tag{S5b}
$$

The boundary conditions Eqs. S2a and S2b (same as Eqs. 3a and 3b in the text) lead $C_4 = -C_2$ and $C_3 = -C_1$. Substituting Eq. S5 for the remaining boundary conditions, we obtain a 6×6 matrix

equation,

$$\begin{pmatrix} M_{11} & M_{12} & \dots & M_{16} \\ M_{21} & M_{22} & \dots & M_{26} \\ \vdots & \vdots & \ddots & \vdots \\ M_{61} & M_{62} & \dots & M_{66} \end{pmatrix} \begin{pmatrix} C_1 \\ C_2 \\ D_1 \\ D_2 \\ D_3 \\ D_4 \end{pmatrix} = \mathbf{0}. \tag{S6}$$

The elements of the matrix $[M]$ in Eq. 8 are given by,

$$M_{11} = -\alpha \frac{h}{2} \left(\cos(\alpha L) - \cosh(\alpha L)\right),$$

$$M_{12} = -\alpha \frac{h}{2} \left(-\sin(\alpha L) - \sinh(\alpha L)\right),$$

$$M_{13} = M_{15} = M_{24} = M_{26} = M_{33} = M_{34} = M_{35} = M_{36} = M_{51} = M_{52} = M_{61} = M_{62} = 0,$$

$$M_{14} = M_{16} = 1,$$

$$M_{21} = -\alpha \left(\cos(\alpha L) - \cosh(\alpha L)\right),$$

$$M_{22} = -\alpha \left(-\sin(\alpha L) - \sinh(\alpha L)\right),$$

$$M_{23} = M_{25} = \beta,$$

$$M_{31} = E_q I_q \alpha^3 \left(-\cos(\alpha L) - \cosh(\alpha L)\right) + M_{tip}\omega^2 \left(\sin(\alpha L) - \sinh(\alpha L)\right)$$
$$+ M_{tip}\omega^2 \frac{d}{2} \alpha \left(\cos(\alpha L) - \cosh(\alpha L)\right),$$

$$M_{32} = E_q I_q \alpha^3 \left(\sin(\alpha L) - \sinh(\alpha L)\right) + M_{tip}\omega^2 \left(\cos(\alpha L) - \cosh(\alpha L)\right)$$
$$+ M_{tip}\omega^2 \frac{d}{2} \alpha \left(-\sin(\alpha L) - \sinh(\alpha L)\right),$$

$$M_{41} = -E_q I_q \alpha^2 \left(-\sin(\alpha L) - \sinh(\alpha L)\right) + \frac{d}{2} M_{tip}\omega^2 \left(\sin(\alpha L) - \sinh(\alpha L)\right)$$
$$+ \left(\left(\frac{d}{2}\right)^2 M_{tip} + I_a\right) \omega^2 \alpha \left(\cos(\alpha L) - \cosh(\alpha L)\right),$$

$$M_{42} = -E_q I_q \alpha^2 \left(-\cos\left(\alpha L\right) - \cosh\left(\alpha L\right)\right) + \frac{d}{2} M_{tip} \omega^2 \left(\cos\left(\alpha L\right) - \cosh\left(\alpha L\right)\right)$$

$$+ \left(\left(\frac{d}{2}\right)^2 M_{tip} + I_a\right) \omega^2 \alpha \left(-\sin\left(\alpha L\right) - \sinh\left(\alpha L\right)\right),$$

$$M_{43} = \left(I_c + \frac{1}{4} l_c M_c \left(l_b + \frac{h}{2} + \frac{1}{4} l_c\right)\right) \omega^2 \beta \cos\left(\beta l_b\right) + \left(l_b + \frac{h}{2} + \frac{1}{4} l_c\right) M_c \omega^2 \sin\left(\beta l_b\right)$$

$$+ \rho_w A_w \omega^2 \left(-\frac{1}{\beta}\left(l_b + \frac{h}{2}\right) \cos\left(\beta l_b\right) + \frac{1}{\beta^2} \sin\left(\beta l_b\right) + \frac{h}{2\beta}\right),$$

$$M_{44} = -\left(I_c + \frac{1}{4} l_c M_c \left(l_b + \frac{h}{2} + \frac{1}{4} l_c\right)\right) \omega^2 \beta \sin\left(\beta l_b\right) + \left(l_b + \frac{h}{2} + \frac{1}{4} l_c\right) M_c \omega^2 \cos\left(\beta l_b\right)$$

$$+ \rho_w A_w \omega^2 \left(\frac{1}{\beta}\left(l_b + \frac{h}{2}\right) \sin\left(\beta l_b\right) + \frac{1}{\beta^2} \cos\left(\beta l_b\right) - \frac{1}{\beta^2}\right),$$

$$M_{45} = \left(I_c + \frac{1}{4} l_c M_c \left(l_b + \frac{h}{2} + \frac{1}{4} l_c\right)\right) \omega^2 \beta \cosh\left(\beta l_b\right) + \left(l_b + \frac{h}{2} + \frac{1}{4} l_c\right) M_c \omega^2 \sinh\left(\beta l_b\right)$$

$$+ \rho_w A_w \omega^2 \left(\frac{1}{\beta}\left(l_b + \frac{h}{2}\right) \cosh\left(\beta l_b\right) - \frac{1}{\beta^2} \sinh\left(\beta l_b\right) - \frac{h}{2\beta}\right),$$

$$M_{46} = \left(I_c + \frac{1}{4} l_c M_c \left(l_b + \frac{h}{2} + \frac{1}{4} l_c\right)\right) \omega^2 \beta \sinh\left(\beta l_b\right) + \left(l_b + \frac{h}{2} + \frac{1}{4} l_c\right) M_c \omega^2 \cosh\left(\beta l_b\right)$$

$$+ \rho_w A_w \omega^2 \left(\frac{1}{\beta}\left(l_b + \frac{h}{2}\right) \sinh\left(\beta l_b\right) - \frac{1}{\beta^2} \cosh\left(\beta l_b\right) + \frac{1}{\beta^2}\right),$$

$$M_{53} = \left(-E_w I_w \beta^3 + \frac{1}{4} l_c M_c \omega\ 2\beta\right) \cos\left(\beta l_b\right) + M_c \omega^2 \sin\left(\beta l_b\right),$$

$$M_{54} = \left(E_w I_w \beta^3 - \frac{1}{4} l_c M_c \omega\ 2\beta\right) \sin\left(\beta l_b\right) + M_c \omega^2 \cos\left(\beta l_b\right),$$

$$M_{55} = \left(E_w I_w \beta^3 + \frac{1}{4} l_c M_c \omega\ 2\beta\right) \cosh\left(\beta l_b\right) + M_c \omega^2 \sinh\left(\beta l_b\right),$$

$$M_{56} = \left(E_w I_w \beta^3 + \frac{1}{4} l_c M_c \omega\ 2\beta\right) \sinh\left(\beta l_b\right) + M_c \omega^2 \cosh\left(\beta l_b\right),$$

$$M_{63} = \left(E_w I_w \beta^2 + \frac{1}{4} l_c M_c \omega^2\right) \sin\left(\beta l_b\right) + \left(\left(\frac{1}{4} l_c\right)^2 M_c + I_c\right) \omega^2 \cos\left(\beta l_b\right),$$

$$M_{64} = \left(E_w I_w \beta^2 + \frac{1}{4} l_c M_c \omega^2\right) \cos\left(\beta l_b\right) - \left(\left(\frac{1}{4} l_c\right)^2 M_c + I_c\right) \omega^2 \sin\left(\beta l_b\right),$$

$$M_{65} = \left(-E_w I_w \beta^2 + \frac{1}{4} l_c M_c \omega^2\right) \sinh\left(\beta l_b\right) + \left(\left(\frac{1}{4} l_c\right)^2 M_c + I_c\right) \omega^2 \cosh\left(\beta l_b\right),$$

$$M_{66} = \left(-E_w I_w \beta^2 + \frac{1}{4} l_c M_c \omega^2\right) \cosh(\beta l_b) + \left(\left(\frac{1}{4} l_c\right)^2 M_c + I_c\right) \omega^2 \sinh(\beta l_b).$$

All elements of the matrix M_{ij} shown here are functions of α and β. According to Eq. S5, they can be represented only by functions of the angular frequency ω. For a non-trivial solution to exist, the determinant of the coefficient matrix in Eq. S6 should be equal to zero. The countably infinite solutions for ω derived from the equation,

$$\det M = 0. \tag{S7}$$

Note that it is very difficult to obtain an explicit formula for the roots of Eq. S7, but we can easily find the roots by examining the zero crossings of the plot of the left-hand term of the equation with respect to ω. The roots of Eq. S7 correspond to the eigenfrequencies of the qPlus sensor, $f_i = \omega_i / 2\pi \, (i = 1, 2, 3...)$. The shape of the eigenmode was determined via Eq. S5 with the coefficients corresponding to the eigenfrequency, $C_1 \cdots D_4$, derived from Eq. S6.

S2 FEM results

Figure S1 shows finite element method (FEM) results of the first, second, and third eigenmodes of the qPlus sensors with the probe length of 1.4, 1.7, and 2.0 mm. The simulation was carried out with the physical parameters listed in Table 1 using 3D CAD software (FreeCAD) as previously described[1]. The shape of the eigenmodes obtained by the simulation was in good agreement with the theoretical results shown in Fig. 4.

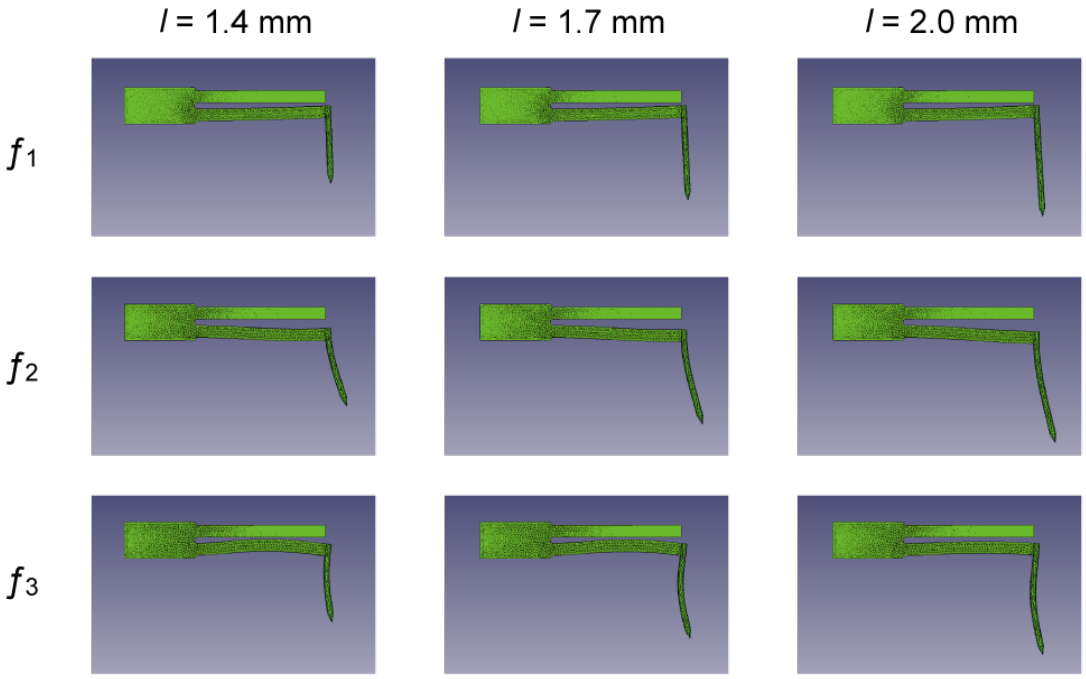

Fig. S1 The FEM results of the first, second, and third eigenmodes of the qPlus sensors with the probe length of 1.4, 1.7, and 2.0 mm.

S3 Sensor charactarization

Figures S2a and S2b show thermal noise spectra of the qPlus sensor used in the experiment around its f_1 and f_3 obtained at the sample temperature of 25°C and 125°C. We should note that the temperature of the qPlus sensor was not certainly known when the sample temperature was 125°C because the sensor was not in contact with the heater but was mildly heated. Both eigenfrequencies are slightly negatively shifted at the sample temperature of 125°C because the eigenfrequency of QTFs varies with temperature as an inverted parabola centered around 25°C[2,3]. The sensitivities of the first and third modes were determined from the thermal noise spectra obtained at 25°C in the same way as described in Sec. 3.1. The obtained sensitivities, $S_{v,1,y}$ and $S_{v,3,l}$, were 84 μV pm^{-1} and 110 μV pm^{-1}, respectively. Note that the voltage signal shown in the spectra is 0.65 times lower than the total voltage signal since the input impedance of the spectrum analyzer is 50 Ω and the output impedance of the preamplifier, which is equal to that of OPA227, is 27 Ω.

Figures S2c and S2d show the transfer functions of the qPlus sensor around f_1 and f_3 at the sample temperature of 125°C. There is no "forest of peaks" in the amplitude components of the transfer functions, which can cause instrumental artifacts in the detected signals.

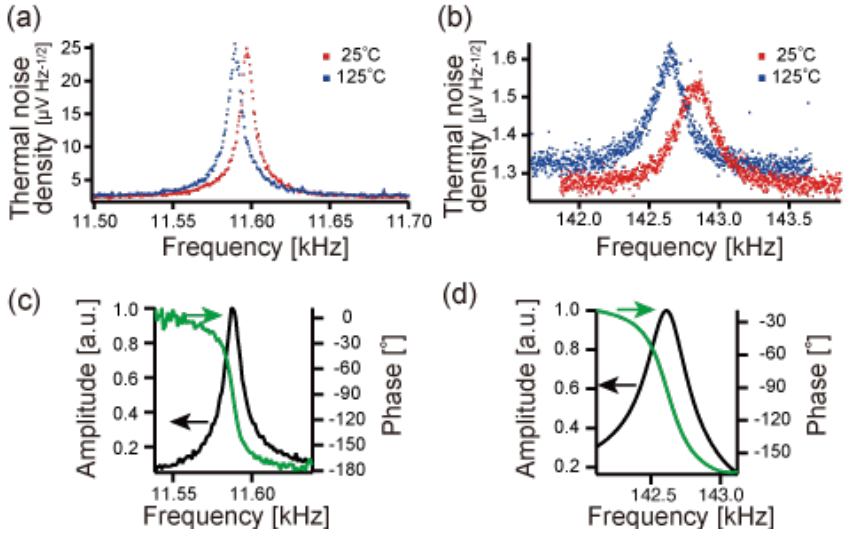

Fig. S2 Thermal noise spectra around the first eigenfrequency (a) and third eigenfrequency (b) of the qPlus sensor used in this experiment ($l = 1.61$ mm, $l_c = 0.17$ mm). The spectra were taken at the sample temperature of 25°C (red points) and 125°C (blue points). Transfer functions of the first mode (c) and third mode (d) of the qPlus sensor measured at the sample temperature of 125°C. The black and green lines show the normalized amplitude and phase of the qPlus sensor.

S4 Bimodal AFM results

Figure S3 shows the bimodal AFM images (topography, E_1, A_3, and ϕ_3) obtained on the P(VDF-TrFE) film at the sample temperature of 125 °C. Energy dissipation in the third mode E_3 (shown in Fig. 10d in the text) is derived from A_3 and ϕ_3 along with the equation given by[4],

$$E_3 = \frac{\pi k_3 A_3^2 f_d}{Q_3}\left(\frac{A_{3,0}}{A_3}\sin(-\phi_3) - \frac{f_d}{f_3}\right), \tag{S8}$$

where f_d, Q_3, and $A_{3,0}$ are the driving frequency, the quality factor, and the free amplitude of the third mode.

The signals of the third mode, A_3 and ϕ_3, gradually drifted in the slow scan direction (y direction). As a result, E_3 also gradually changed in the same direction (shown in Fig. 10d in the text). It assumes that the sensor was being heated during the imaging, which caused the shift of the eigenfrequencies and the variation of the quality factors. It reproducibly occurs even after heating for 1 h before approaching and keeping in the imaging condition for over 1 h. Thus, we compared E_3 at the same y position in the discussion in the text.

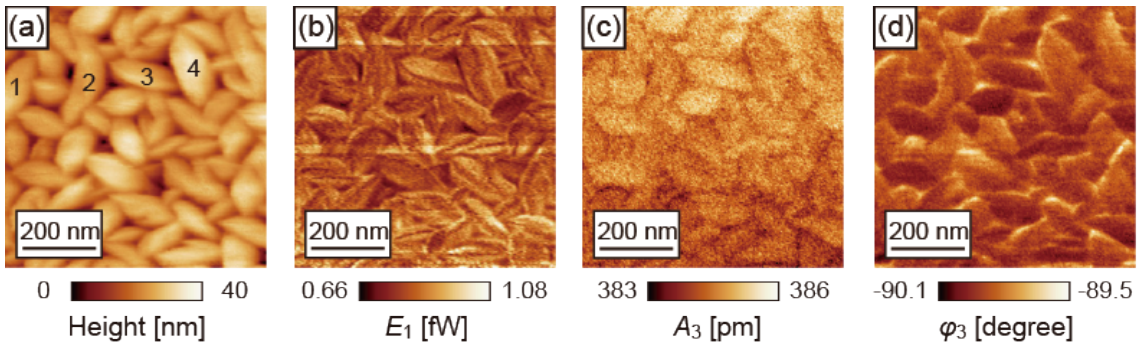

Fig. S3 The bimodal AFM results on the P(VDF-TrFE) film obtained at 125°C under an ambient condition. (a) Topography. (b) Energy dissipation in the first mode E_1. (c) Amplitude of the third mode A_3. (d) Phase of the third mode ϕ_3. The probe length l and the etched part length l_c were 1.61 mm and 0.17 mm, respectively. $f_1 = 11.6$ kHz, $Q_1 = 1600$, $k_{1,y} = 1.9$ kN m^{-1}, $\theta_1 = 41.7°$, $A_1 = 118$ pm, $f_3 = 142.6$ kHz, $Q_3 = 550$, $k_{3,l} = 58.6$ kN m^{-1}, $\theta_3 = 6.3°$, $A_{3,0} = 386$ pm. These images were taken at $\Delta f_1 = +3.5$ Hz.

Figure S4a shows the interaction stiffness in the third mode $k_{int,3}$ derived from A_3 and ϕ_3 shown in Figs. S3c and S3d. $k_{int,3}$ was obtained by the equation shown below[5],

$$k_{int,3} = \frac{k_3 A_{3,0}}{Q_3 A_3} \cos(-\phi_3). \tag{S9}$$

$k_{int,3}$ increased between the grains because of the topographic effects, which is the same as we already pointed out about E_3 in the text. Figure S4b shows a line profile of $k_{int,3}$ on the black line in Figure S4a. The short axis of the grains 1-4 indicated in the topographic image shown in Fig. S3a, which corresponds to the molecular chain orientation, tilt 66°, 84°, -12°, and -81° from the tip oscillation direction at f_3, respectively. The gray-colored zones in the line profiles (Fig. S4b) correspond to the numbered grains. The line profile indicated the relationship of $k_{int,3}$ between the numbered grains as $k_{int,3}^{grain2(84^\circ)} \simeq k_{int,3}^{grain4(-81^\circ)} > k_{int,3}^{grain1(66^\circ)} > k_{int,3}^{grain3(-12^\circ)}$. The conservative tip-sample interactions detected in the third mode $k_{int,3}$ decreased when the tip oscillated parallel to the molecular chain orientation of the P(VDF-TrFE); that is, the anisotropy of conservative lateral interactions on the P(VDF-TrFE) thin film was also detected. This result indicated that the conservative lateral tip-sample interactions were detected by the third mode of the qPlus sensor with a long probe.

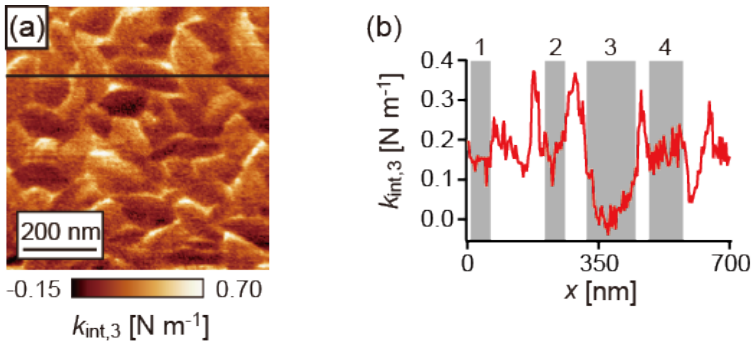

Fig. S4 (a) Interaction stiffness in the third mode $k_{int,3}$ calculated from A_3 and ϕ_3 shown in Figs. S3c and S3d, along with Eq. S9. (b) Line profile of $k_{int,3}$ on the black line in (a).

Notes and references

1 Y. Yamada, T. Ichii, T. Utsunomiya and H. Sugimura, *Japanese Journal of Applied Physics*, 2019, **58**, 095003.

2 E. Momosaki, Proceedings of International Frequency Control Symposium, 1997, pp. 552–565.

3 F. J. Giessibl, *Review of Scientific Instruments*, 2019, **90**, 011101.

4 J. P. Cleveland, B. Anczykowski, A. E. Schmid and V. B. Elings, *Applied Physics Letters*, 1998, **72**, 2613–2615.

5 A. J. Katan, M. H. van Es and T. H. Oosterkamp, *Nanotechnology*, 2009, **20**, 165703.